

2.E Multiple X-Ray Diffraction in Crystals: Application to Two-Dimensional Imaging and Low-Loss Transmission

Applications of multiple x-ray diffraction in crystals was the subject of a proposal to the National Laser Users Facility by **Professor Ben Post** of the Polytechnic Institute of New York, in collaboration with LLE. Some results of the ensuing work are described here.

The major goals of this investigation were (a) the development of a method for two-dimensional imaging of x rays using simultaneous n-beam diffraction within crystals, and (b) the application of the above to the study of the stability of laser-irradiated spherical targets by imaging x-ray line emission from thin metallic layers embedded within plastic shell targets. We have used such diffraction to image test objects and to demonstrate the possibility of achieving satisfactory spatial resolution; these techniques will be used to image target emission.

In addition to imaging, simultaneous diffraction of x rays within crystals makes possible other applications. One involves the substantial reduction of x-ray absorption along directions that satisfy diffraction conditions with respect to several sets of crystal planes. We have demonstrated such reduction in absorption for various cases of simultaneous diffraction in germanium. Such reduction can be crucial for the successful operation of a gamma-ray laser.

Monochromatic Imaging Using Simultaneous Diffraction of X Rays by Crystals

One-dimensional imaging in the direction of dispersion is always obtained in Bragg diffraction from plane crystals. The spatial resolution (i.e., the minimum resolvable element Δx) is obtained by differentiating the Bragg equation, in first order:

$$2d\sin\theta = \lambda, \quad (1)$$

to obtain

$$2d\cos\theta\Delta\theta = \Delta\lambda. \quad (2)$$

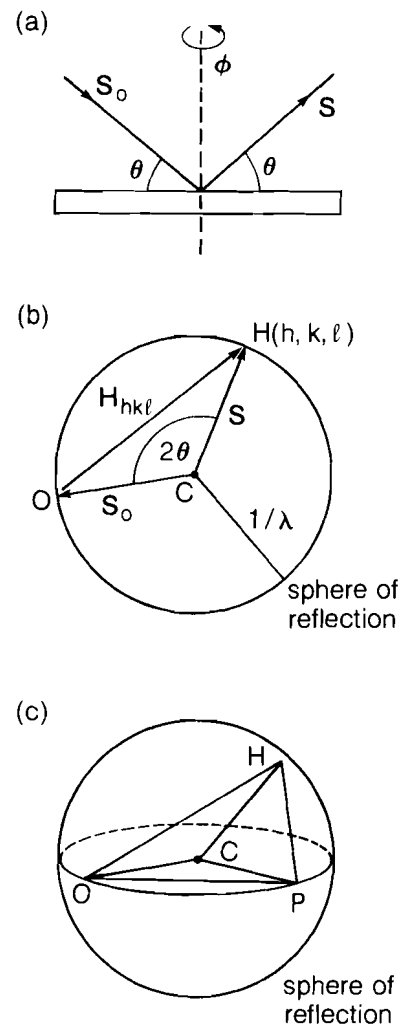
Since the resolvable element Δx is related to the angular spread $\Delta\theta$ through $\Delta x = L\Delta\theta$, where L is the total distance traveled by the diffracted beam from the source to the detector, therefore

$$\Delta x = L \operatorname{tg}\theta(\Delta\lambda/\lambda). \quad (3)$$

In typical laser-target experiments, this spatial resolution is in fact limited by the spectral width rather than by the crystal properties. As a typical

example, we select the Ti^{+20} resonance line at 2.62 \AA and assume the laser plasma source to have an ion temperature of 1 keV . The line width will be mostly due to the Doppler effect (with some additional opacity broadening possible), so that $\Delta\lambda/\lambda = 3.5 \times 10^{-4}$, yielding a spatial resolution of $20 \text{ }\mu\text{m}$ at $L = 10 \text{ cm}$. In a direction perpendicular to that of the dispersion there is no imaging at all, and the diffracted beam from a divergent source has the shape of a thin cone for a given wavelength.

Simultaneous diffraction, by contrast, can provide two-dimensional imaging.¹ The principles of simultaneous diffraction are described in Fig. 28.18. For a monochromatic incident beam, θ is adjusted to the Bragg angle for diffraction from the planes parallel to the surface. If the crystal is rotated around the ϕ axis, diffraction peaks are generated (as shown in Fig. 28.19), even when the primary reflection has zero



E3962

Fig. 28.18

Schematic of simultaneous diffraction:

- (a) monochromatic incident beam, in which θ is adjusted to the Bragg angle of diffraction from the planes parallel to the surface, and the ϕ rotation brings multiple diffraction peaks into diffraction,
 (b) Bragg condition in reciprocal lattice,
 (c) by rotating around OH [ϕ -rotation in (a)], additional reciprocal lattice points like P touch the reflection sphere.

intensity. To understand this, we look at the reciprocal-lattice construction [Fig. 28.18(b)]. S_0 and S are unit vectors in the direction of the incident and diffracted beams, respectively, and θ is the Bragg angle. The Bragg condition is satisfied when the point H lies on the sphere of reflection (the Ewald sphere): diffraction from the planes of Miller indices (hkl) will then occur along the S direction. Rotation of the crystal about the ϕ axis is equivalent to rotating the reciprocal lattice about OH [Fig. 28.18(b)]. During this rotation, many points [such as P in Fig. 28.18(c)] cross the surface of the sphere of reflection and give rise to n-beam diffraction. More than one point can simultaneously cross the surface, giving rise to higher-order n-beam diffraction (e.g., six-beam diffraction). We may say that the incident beam CO in Fig. 28.18(c) is diffracted by the OP planes (i.e., those with Miller indices equal to the coordinates of P), giving rise to a diffracted beam in the CP direction. This beam is also diffracted by the PH planes that are perpendicular to PH and are spaced $1/|HP|$ apart. These yield diffraction in the CH direction. Diffraction is in the same direction (CH) as if diffracted from the planes parallel to the surface (OH). Of course, these two diffractions are simultaneous rather than sequential.

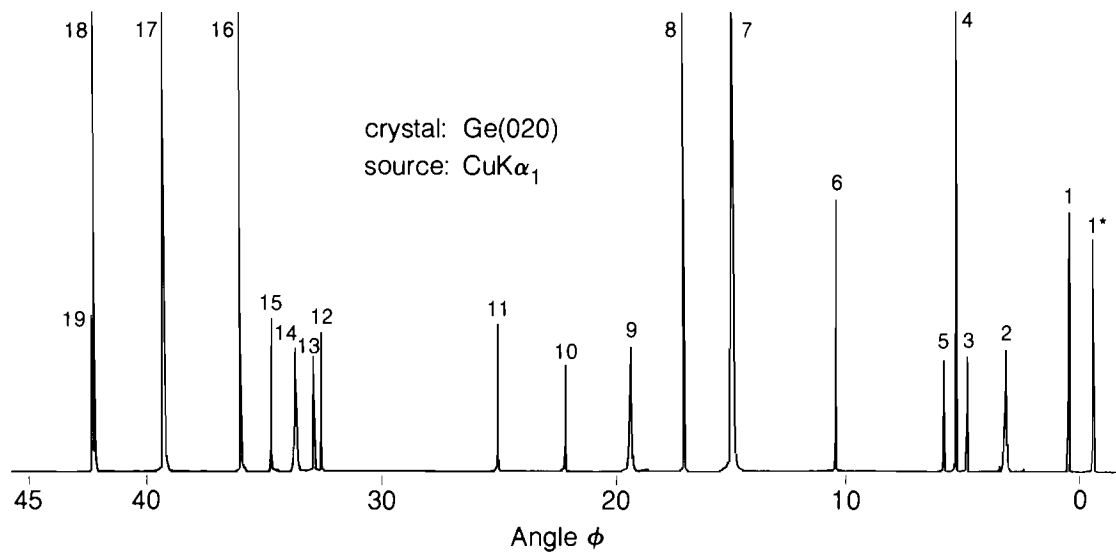
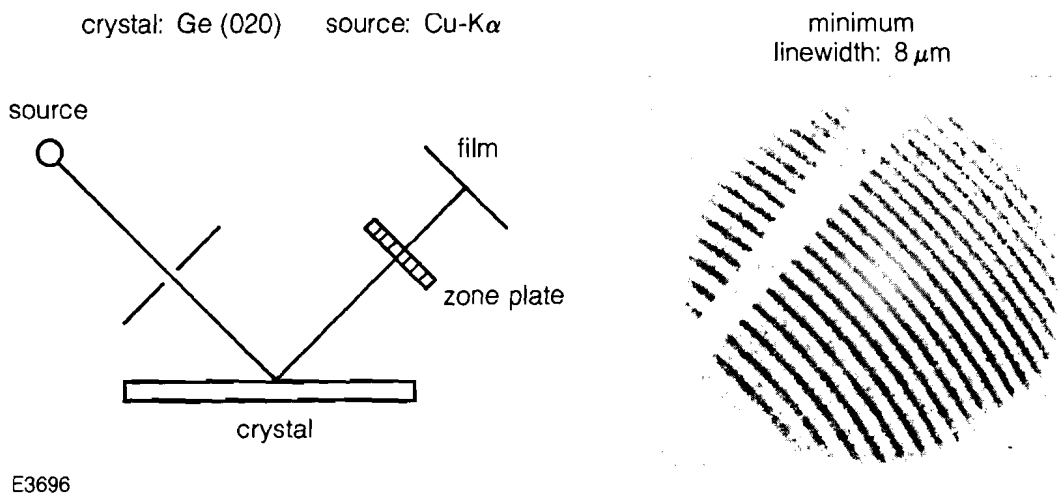


Fig. 28.19
Simultaneous (three-beam) diffraction from the (020) planes of germanium. Source: $K\alpha_1$ line of Cu.

Because two angular conditions (θ and ϕ) have to be satisfied, the diffracted beam is quasi-collimated. It can therefore yield a two-dimensional shadowgraph image, of unit magnification, of any object it traverses or of the emitting object itself. It should be emphasized that multiple diffraction is not limited to the case of zero-structure factor. In the general case, two sets of spectra can appear on the film, with the intersections, enhanced in intensity, corresponding to simultaneous diffraction. The two-beam spectra in this case constitute a background for the n-beam diffraction peaks.

Figure 28.19 shows multiple diffraction spectra obtained with $\text{CuK}\alpha_1$ radiation from an x-ray tube. The angle $\phi = 0$ is chosen so that the spectra are mirror imaged with respect to this point. Some of the peaks extend beyond the height of the figure and are truncated. The peak marked 7 in Fig. 28.19 was chosen for the imaging tests in Figs. 28.20 and 28.21; it corresponds to simultaneous diffraction from the $(\bar{1}3\bar{1})$ and $(1\bar{1}1)$ planes. The three indices add up to (020) . This simply follows from the vector relation $\text{OH} = \text{OP} + \text{PH}$ in Fig. 28.18(c).



E3696

Fig. 28.20
Imaging testing using the simultaneous diffraction peak marked 7 in Fig. 28.19, from Ge (020) planes. A weak and shifted image from the $\text{K}\alpha_2$ line can be seen.

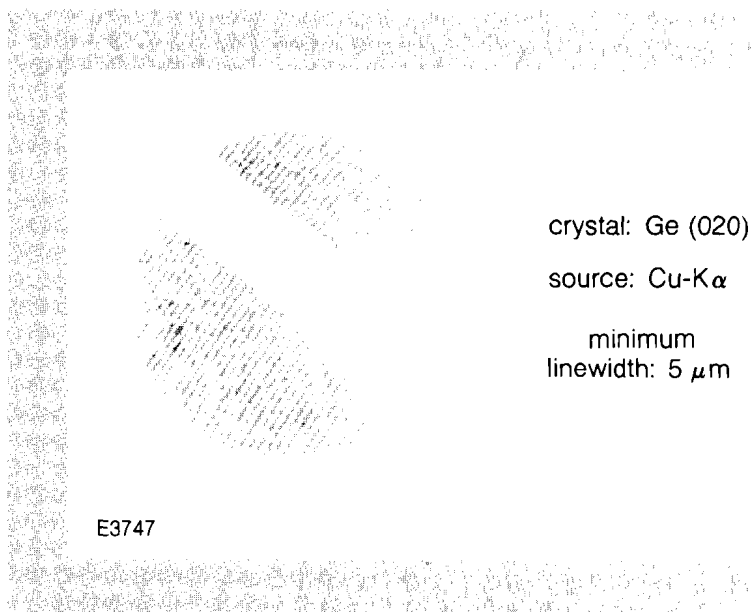


Fig. 28.21
Imaging of a finer-line section of the zone plate, as in Fig. 28.20.

Table 28.III shows the diffracting-plane indices corresponding to the scans in Fig. 28.19. The indices hkl refer to the reciprocal lattice point that passes through the surface of the Ewald sphere during rotation of the crystal. In four-beam cases, two points pass through the surface simultaneously; three points pass in five-beam cases. Azimuthal angle is the angle (relative to some arbitrary standard, such as a mirror plane) at which the point enters or leaves the sphere. Beta is the angular

Table 28.III
Simultaneous n -beam diffraction peaks: Ge (020), $CuK\alpha_1$

	$hk\ell(1)$	$hk\ell(2)$	No. of Beams	Azimuthal Angle	Beta	Azimuthal Angle
1.	$\bar{3}\bar{1}\bar{3}$	$\bar{3}\bar{3}\bar{3}$	4	0.395	-90.79	269.61
2.	$\bar{1}\bar{1}\bar{7}$	---	3	2.42	-21.09	341.32
3.	$\bar{3}\bar{1}\bar{5}$	$3\bar{3}\bar{5}$	4	5.15	51.62	56.78
4.	$3\bar{1}\bar{1}$	---	3	5.38	132.37	137.75
5.	$\bar{3}\bar{1}\bar{5}$	---	3	5.63	-73.18	292.44
6.	$\bar{3}\bar{1}\bar{3}$	---	3	10.36	-110.71	259.64
7.	$\bar{1}\bar{3}\bar{1}$	$\bar{1}\bar{1}\bar{1}$	4	14.90	-119.79	255.11
8.	$3\bar{1}\bar{1}$	$3\bar{3}\bar{1}$	4	17.24	108.65	125.89
9.	$1\bar{1}\bar{7}$	---	3	18.68	-21.09	357.58
10.	$5\bar{1}\bar{3}$	---	3	22.44	73.18	95.63
11.	$\bar{1}\bar{3}\bar{5}$	$\bar{1}\bar{1}\bar{5}$	4	24.90	-72.42	312.48
12.	$5\bar{1}\bar{1}$	---	3	32.76	91.85	124.62
13.	$5\bar{1}\bar{3}$	$5\bar{3}\bar{3}$	4	33.22	51.62	84.85
14.	$5\bar{1}\bar{5}$	---	3	34.45	21.09	55.55
15.	$\bar{1}\bar{1}\bar{5}$	---	3	34.62	-91.85	302.76
16.	$\bar{1}\bar{3}\bar{3}$	$\bar{1}\bar{1}\bar{3}$	4	35.89	-108.65	287.24
17.	$\bar{1}\bar{1}\bar{1}$	---	3	39.24	-168.49	230.76
18.	$3\bar{1}\bar{1}$	---	3	42.25	132.37	174.62
19.	$5\bar{3}\bar{1}$	$5\bar{1}\bar{1}$	4	42.48	72.42	114.90

Diffraction peaks obtained when rotating the crystal around the normal to the (020) planes. The Bragg angle with respect to these planes is maintained while the azimuthal angle changes. For each diffraction peak, the table shows the coordinates of the reciprocal lattice point(s) whose passage through the surface of the sphere of reflection gives rise to that peak. The two azimuthal angles correspond to either entering or leaving the reflection sphere. Beta is the difference between these two angles. For negative beta, the first angle corresponds to exit; for positive beta, it corresponds to entry.

interval between entry and exit of the sphere. If beta is negative, the first azimuthal angle (in column 4) refers to emergence from the sphere, and the second azimuthal angle (in column 6) to entry; if beta is positive, the above are reversed.

Figures 28.20 and 28.21 show imaging test results obtained with $\text{CuK}\alpha$ radiation. A freestanding gold zone plate was chosen as a test object to be imaged by shadowgraphy onto a high-resolution film (Kodak RAR-2497). The 0.5-mm pinhole limits the image size and reduces some background, but has no effect on the imaging. The smallest zone plate linewidth in Fig. 28.20 is $8\ \mu\text{m}$, and in Fig. 28.21 it is $5\ \mu\text{m}$. This is an indication of the spatial resolution achievable in a direction perpendicular to that of the dispersion. In these figures, the distance of source to zone plate (along the ray) is 200 cm, and that of the zone plate to film is 2 cm. The source size is about 3 mm, yielding a penumbral shadow of at least $30\ \mu\text{m}$. Clearly, the imaging in these figures is due to the properties of simultaneous diffraction.

The direction of dispersion is seen in Fig. 28.20, as the $\text{K}\alpha_2$ component gives rise to a weak, shifted image with respect to the dominant image. In this direction the spatial resolution is limited by the spectral linewidth, just as in two-beam Bragg diffraction. As shown above, at a total distance of 10 cm this resolution will be typically $20\ \mu\text{m}$. In the perpendicular direction the spatial resolution can only be limited by the crystal properties. For the germanium crystal used, the rocking-curve width is about 10^{-4} , yielding a spatial resolution of $2\ \mu\text{m}$ for the 2-cm imaging distance in Fig. 28.20. This agrees with Fig. 28.21, which indicates a resolution better than $5\ \mu\text{m}$. In this case, the zone plate was rotated by about 90° , to demonstrate the resolution perpendicular to the direction of dispersion. For a total distance of 10 cm from a laser target to the crystal, then to the film, a $10\text{-}\mu\text{m}$ resolution can be achieved in this direction. Different wavelengths will yield images displaced with respect to each other. As shown here, $10\text{-}\mu\text{m}$ to $20\text{-}\mu\text{m}$ resolution is possible in a two-dimensional image at each wavelength. Such images can be useful in studying instability and mixing in laser target implosions. For this, thin layers of elements like titanium or chromium have to be embedded in the target and isolated, strong x-ray lines from the various layers have to be imaged.

Reduction in Absorption on Multiple-Diffraction Beams

Simultaneous diffraction has other important applications, in addition to imaging:

- (a) In the Laue mode (radiation traversing the crystal), absorption due to the photoelectric effect is greatly reduced² for n-beam diffraction peaks. This is in addition to the reduction in absorption (Borrmann effect) in all two-beam, Laue diffraction. This property is important for designs of gamma-ray lasers where propagation of wavelengths of order $1\ \text{\AA}$ through a relatively large thickness of crystalline material is called for.
- (b) The spectral dispersion in this case has two components: $d\theta/d\lambda$ and $d\phi/d\lambda$. The second dispersion can be much larger than the first, yielding a high-resolution recording of spectra.

- (c) The profiles of n-beam diffraction peaks near the baseline indicate the sign of the phase shift introduced by the diffraction, thereby making possible the experimental determination of x-ray reflection phases from diffraction data.³

The multiple diffraction described above was measured in reflection (or Bragg diffraction), whereas the reduction in absorption described here was measured in transmission (or Laue diffraction). The principles of resonant x-ray beams in crystals (i.e., multiple diffraction) are essentially the same in both cases. However, for the determination of absorption the transmission case is the more relevant.

We show in Fig. 28.22 the geometry used in the Laue case. In the measurements leading to Fig. 28.19, the crystal had to be rotated in order to scan the peaks of multiple diffraction, whereas here we used film to record simultaneously the diffracted beams in a range of directions. In Fig. 28.19 the incident beam needs to be collimated; here, we use a divergent beam, placing a micro-focus source (0.1x0.1 mm) close to the crystal (7 cm). The film is placed far from the crystal (200 cm) to increase the ratio of signal to scattered background and to avoid broadening due to the source size.

Other characteristic differences between the results obtained in this and the previous subsection will be noted. As Fig. 28.22 shows, in conventional Laue diffraction there are two beams that leave the crystal: the forward-diffracted beam, which travels in the same direction as the incident beam (except for a slight shift that depends on the crystal thickness and the Bragg angle); the transmitted-reflected beam, which is analogous to the one diffracted beam in the case of Bragg diffraction.

In the experiments described in the previous subsection, the Bragg angle with respect to the planes parallel to the crystal surface corresponded to a so-called forbidden diffraction (i.e., having a zero structure-factor). Therefore, diffracted beams were observed only in directions corresponding to multiple diffraction. In Fig. 28.22, the divergent beam can give rise to two-beam Laue diffraction, which will

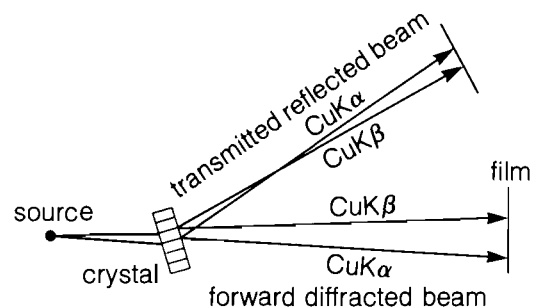


Fig. 28.22
Laue (transmission) geometry for measuring multiple-diffraction peaks.

appear on film as lines in the plane of the figure. Diffracting planes other than those shown in Fig. 28.22 will yield lines in different orientations. The transmitted-reflected beam may also satisfy the diffraction condition with respect to a second set of planes. This will be evidenced by an *enhancement* at one point along the line, mainly due to the theoretically predicted reduction in absorption. For the forward-diffracted beam this point of enhancement is observed at the intersection of two lines on the film, from the two two-beam interactions.

Figures 28.23 and 28.24 show examples of results obtained with the geometry of Fig. 28.22, where radiation from a copper-anode tube is transmitted through a 0.5-mm-thick germanium crystal.

Figure 28.23 shows the enhancement due to reduction in absorption at the intersection points of pairs of forward-diffracted beams (lower right). Also, it shows n-beam enhancement points on transmitted-reflected beams (upper and left features).

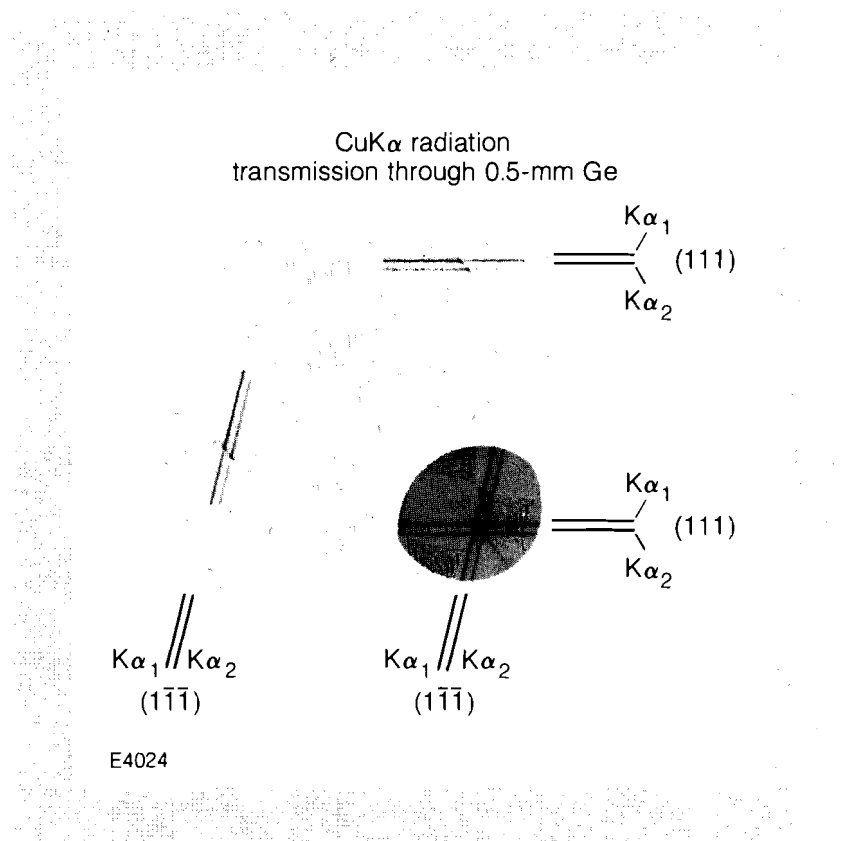


Fig. 28.23
Three-beam diffraction (at enhanced-intensity points).

Figure 28.24 shows a four-beam diffraction case, where the four reciprocal lattice points are 000, $1\bar{1}1$, $20\bar{2}$, and $3\bar{1}\bar{1}$. The four points are coplanar. The divergent incident beam enables the observation of $3\bar{1}\bar{1}$ diffraction lines due to CuK α_1 , K α_2 , and CuK β , as well as four-beam enhancements at these wavelengths. The vertical streak that passes through the K α_1 , K α_2 , and K β four-beam points is due to the four-beam enhancement of the very faint continuum of wavelengths between K α and K β . Theory shows that when a larger number of interactions

occur simultaneously, the reduction in absorption is more pronounced. In a six-beam case in germanium, the linear absorption coefficient for three of the modes (for 1.54-Å radiation) is calculated⁴ to be less than 1 cm^{-1} (there are 12 modes when polarization is included). The absorption in other modes ranges up to 690 cm^{-1} . The total attenuation through a thickness of a few millimeters should therefore be very small. A quantitative determination of these values will be the subject of continuing work.

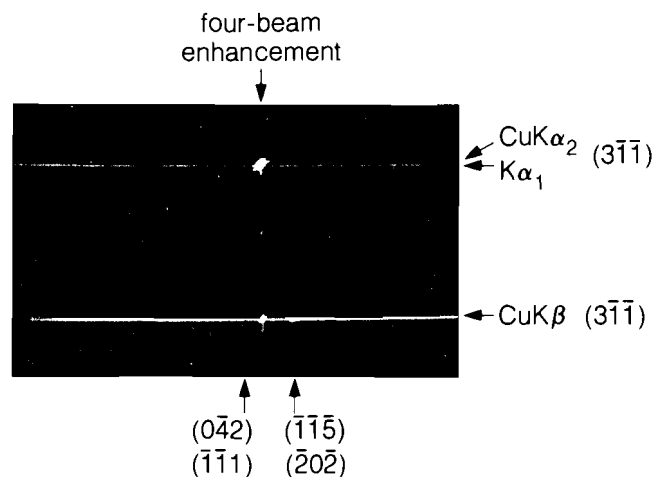


Fig. 28.24
Four-beam diffraction (at enhanced-intensity points). The vertical line is enhanced, four-beam diffraction of the continuum.

ACKNOWLEDGMENT

This work was supported by the U.S. Department of Energy Office of Inertial Fusion under agreement No. DE-A508-84DP40197 with the Polytechnic Institute of New York and by the National Laser Users Facility at the University of Rochester Laboratory for Laser Energetics under agreement No. DE-FC08-85DP40200.

REFERENCES

1. B. S. Fraenkel, *Appl. Phys. Lett.* **36**, 341 (1980); **41**, 234 (1982).
2. B. Post, S. L. Chang, and T. C. Huang, *Acta. Crystallogr. Sect. A*: **33**, 90 (1977); B. Post, *ibid.* **39**, 711 (1983); B. Post, J. Nicholosi, and J. Ladell, *ibid.* **40**, 684 (1984).
3. B. Post, *Phys. Rev. Lett.* **39**, 760 (1977).
4. T. C. Huang, M. H. Tillinger, and B. Post, *Z. Naturforsch.* **28a**, 600 (1973).